Process dependence of H passivation and doping in H-implanted ZnO

Report Documentation Page

1. REPORT DATE **04 JAN 2013**	2. REPORT TYPE	3. DATES COVERED **00-00-2013 to 00-00-2013**

4. TITLE AND SUBTITLE **Process dependence of H passivation and doping in H-implanted ZnO**	5a. CONTRACT NUMBER
	5b. GRANT NUMBER
	5c. PROGRAM ELEMENT NUMBER
6. AUTHOR(S)	5d. PROJECT NUMBER
	5e. TASK NUMBER
	5f. WORK UNIT NUMBER

7. PERFORMING ORGANIZATION NAME(S) AND ADDRESS(ES) **The Ohio State University,Department of Electrical and Computer Engineering,Columbus,OH,43210**	8. PERFORMING ORGANIZATION REPORT NUMBER

9. SPONSORING/MONITORING AGENCY NAME(S) AND ADDRESS(ES)	10. SPONSOR/MONITOR'S ACRONYM(S)
	11. SPONSOR/MONITOR'S REPORT NUMBER(S)

12. DISTRIBUTION/AVAILABILITY STATEMENT
Approved for public release; distribution unlimited

13. SUPPLEMENTARY NOTES
J. Phys. D: Appl. Phys. 46 (2013) 055107 (7pp), Published 4 January 2013,Government or Federal Purpose Rights License

14. ABSTRACT
We used depth-resolved cathodoluminescence spectroscopy (DRCLS), photoluminescence (PL) spectroscopy and temperature-dependent Hall-effect (TDHE) measurements to describe the strong dependence of H passivation and doping in H-implanted ZnO on thermal treatment. Increasing H implantation dose increases passivation of Zn and oxygen vacancy-related defects, while reducing deep level emissions. Over annealing temperatures of 100?400 °C at different times, 1 h annealing at 200 °C yielded the lowest DRCLS deep level emissions highest TDHE carrier mobility, and highest near band-edge PL emission. These results describe the systematics of dopant implantation and thermal activation on H incorporation in ZnO and their effects on its electrical properties.

15. SUBJECT TERMS

16. SECURITY CLASSIFICATION OF:			17. LIMITATION OF ABSTRACT	18. NUMBER OF PAGES	19a. NAME OF RESPONSIBLE PERSON
a. REPORT **unclassified**	b. ABSTRACT **unclassified**	c. THIS PAGE **unclassified**	**Same as Report (SAR)**	**8**	

Process dependence of H passivation and doping in H-implanted ZnO

Z Zhang[1], D C Look[2,3], R Schifano[4], K M Johansen[4], B G Svensson[4] and L J Brillson[1,5,6]

[1] Department of Electrical and Computer Engineering, The Ohio State University, Columbus, OH 43210, USA

[2] Semiconductor Research Center, Wright State University, Dayton, OH 45432, USA

[3] Sensors Directorate, Air Force Research Laboratory, Wright-Patterson Air Force Base, OH 45433, USA

[4] Department of Physics, University of Oslo, PO Box 1048 Blindern, N-0316 Oslo, Norway

[5] Department of Physics, The Ohio State University, Columbus, OH 43210, USA

[6] Center for Materials Research, The Ohio State University, Columbus, OH 43210, USA

E-mail: zhang.720@osu.edu

Abstract

We used depth-resolved cathodoluminescence spectroscopy (DRCLS), photoluminescence (PL) spectroscopy and temperature-dependent Hall-effect (TDHE) measurements to describe the strong dependence of H passivation and doping in H-implanted ZnO on thermal treatment. Increasing H implantation dose increases passivation of Zn and oxygen vacancy-related defects, while reducing deep level emissions. Over annealing temperatures of 100–400 °C at different times, 1 h annealing at 200 °C yielded the lowest DRCLS deep level emissions, highest TDHE carrier mobility, and highest near band-edge PL emission. These results describe the systematics of dopant implantation and thermal activation on H incorporation in ZnO and their effects on its electrical properties.

(Some figures may appear in colour only in the online journal)

1. Introduction

The wide band gap semiconductor ZnO ($E_g \approx 3.4$ eV) is a leading candidate for next generation opto- and micro-electronics due to its high exciton binding energy, thermo-chemical stability, environmental compatibility and potential applications for light-emitting devices and photovoltaics [1, 2]. As-grown un-doped ZnO is naturally n-type, usually attributed to native defects [3, 4] and/or various donor impurities, such as Al, In, H [5–7]. However, the origin of the n-type conductivity is still controversial, and the ability to understand and control the electrical behaviour of intrinsic and impurity related defects in ZnO remains a fundamental, unresolved challenge. Hydrogen is one of the most common but important impurities during various synthesis processes of ZnO [8, 9]. It could contribute to n-type ZnO conductivity by passivating ionized compensating acceptors [10–15] or acting as shallow donors [7, 16–24]. Previous theoretical studies predicted that H is likely to passivate zinc vacancy (V_{Zn}) and substitutional lithium on zinc site (Li_{Zn}) defects by forming neutral X_{Zn}–H complexes [13, 14], and the H passivation of acceptor defect states have been confirmed by photoluminescence (PL) spectroscopy [10, 11], infrared (IR) absorption spectroscopy [12] and positron annihilation spectroscopy (PAS) [15]. Different local vibrational modes in the IR spectra were related to different hydrogen-related defects in ZnO [12, 25–27]. Hydrogen is also a shallow donor in ZnO according to first-principles calculations [7, 17], confirmed experimentally [9, 16, 18–24]. Various experiments identify two types of H donors: (1) a bound exciton emission peak described as I_4 in PL spectroscopy [19, 20], which was later identified as hydrogen bound with an oxygen vacancy [24], H_O, consistent with Janotti and Van de Walle's theory [7]; (2) hydrogen at the bond-centred interstitial site [24], H_{BC} from IR absorption spectroscopy [12]. Moreover, H has also been suggested for possible p-type fabrication by improving acceptor solubility through forming H-acceptor complexes [13]. Here we present results aimed at understanding the influence of dopant implantation and thermal activation on H incorporation in ZnO in order to control its electrical properties.

Based on combined depth-resolved cathodoluminescence spectroscopy (DRCLS), PAS and other surface science techniques, our previous work correlated the commonly observed 1.9–2.1 eV 'red' and 2.3–2.5 eV 'green' luminescence with zinc vacancies and vacancy clusters (denoted $(V_{Zn})_n$-related) and oxygen vacancy (V_O)-related defects, respectively [28]. PAS and secondary ion mass spectrometry (SIMS) profiles demonstrate that, compared with V_{Zn}, the Li_{Zn} acceptor is the dominant trap for H in hydrothermally grown (HT-) ZnO [29]. H implantation could form an n^+-layer in ZnO due to H donor and implantation-induced defects [22]. It has also been shown that the H is trapped in ZnO for temperatures below 250 °C [30]. Moreover, temperature-dependent Hall-effect (TDHE) measurements show that 200 °C annealing in Ar after H implantation results in the highest carrier mobility [31, 32]. However, the implantation and thermal dependence of H incorporation and its electrical behaviour in ZnO is still under debate.

In this work, we report on the passivation and donor effect of ion-implanted H with various concentrations up to 3×10^{18} cm^{-3} in single-crystal bulk hydrothermal (HT) ZnO. We correlated deep band DRCLS emission intensities with implanted H concentration, the thermal process dependence of defect-H passivation, and the resultant electrical properties of H-implanted ZnO. From combined experiments, we summarize optimal annealing conditions for H doping and defect passivation.

2. Experimental

Six n-type HT-ZnO wafers with a size of $10 \times 10 \times 0.5$ mm^3 were used in the study. They are labelled HR, H1, H2, H3, H4 and HH4. HR represents as-grown high resistivity HT-ZnO, while H1–H4 specimens were HT-ZnO implanted on the O face at room temperature (RT) with multiple H$^+$ beam energies to produce approximately box-like profiles of different H concentrations, shown by the simulated profiles in figure 1 using the SRIM-code [33]. The as-grown HT-ZnO has unintentionally doped high Li background concentration $((1–5) \times 10^{17}$ Li cm$^{-3})$ and high resistivity (1–10 kΩ cm) due to self-compensation and the low energy barrier for Li to switch between interstitial and substitutional sites [14, 34]. One quarter of each wafer (HR-3, H1-3, H2-3, H3-3 and H4-3) was heat treated from annealing temperature (T_A) 100 °C to 400 °C in 100 °C steps, with DRCL spectra acquired after each annealing step. In the annealing process, the temperature rose from RT to set temperature (100 °C, 200 °C, 300 °C or 400 °C) in 30 min, and kept at set temperature for 1 h. Annealing at different times was carried out on another H-implanted ZnO HH4, which has same H implantation dose as H4. HH4 was annealed at 200 °C, 300 °C and 400 °C for 30 min, 1 h, 2 h and 4 h, respectively. Two quarters of HR, H2, and H4 wafers received annealing treatments in different sequences: they were first annealed at 100 °C (HR-1, H2-1 and H4-1) and 200 °C (HR-2, H2-2 and H4-2), and then annealed at 300 °C (HR-1, H2-1 and H4-1) and 400 °C (HR-2, H2-2 and H4-2). TDHE and PL features were measured for these specimens after each annealing.
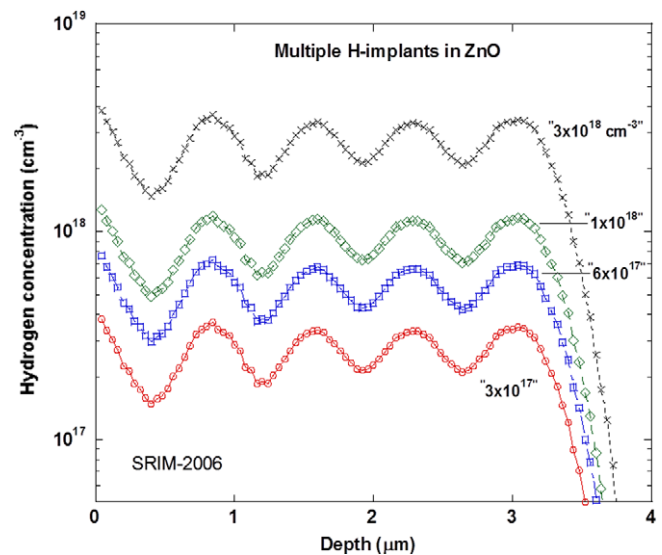

Figure 1. Simulated profile of H concentration in ZnO after H implantation using the SRIM-2006 code. The H concentrations are box profiles extending to depths of ~3.5 µm.

DRCLS measurements were obtained on ZnO $(0\,0\,0\,-\bar{1})$ faces at 80 K in ultrahigh vacuum. See [35, 36] for DRCLS experiment details. Monte Carlo simulation [37] provides depth distributions of the electron–hole pairs generated by the incident electron beam versus E_B. For incident energy $E_B = 1$, 2, 3, 4 and 5 keV, electron–hole pair excitation is maximum at $U_0 = 7$, 18, 32, 50 and 72 nm, respectively. The energy power of the incident beam was $P_B = 2$ mW with a spot diameter of 0.5 mm. References [38, 39] provide descriptions of the TDHE and PL measurements.

3. Results

3.1. Deep band defect passivation with H implantation

Figure 1 shows the simulated profile of H concentration as a function of depth for samples H1, H2, H3 and H4. The multiple H-implantations in each sample produce box areas of roughly constant H concentration: 3×10^{17} cm^{-3}(H1), 6×10^{17} cm^{-3}(H2), 1×10^{18} cm^{-3}(H3) and 3×10^{18} cm^{-3} (H4) that extend to depths of ~3.5 µm. $E_B = 5$ keV CL spectra in figure 2 display the evolution of defect emissions with increasing H implantation dose. Each CL spectrum was normalized relative to its near band-edge (NBE) emission intensity. Figure 2 shows that the deep band emissions at ~2.06 eV and ~2.50 eV both decrease with increasing H implantation dose. A minor exception to this trend is H2, which also deviated in other trends as well. Overall, the highest H dose corresponds to the lowest deep band emission, which suggests that the implanted H passivates not only the Zn vacancy, but also the oxygen vacancy. Figure 2 illustrates that the passivation effect increases with increasing H implantation dose. The inset in figure 2 displays the evolution of deconvolved broad deep level emission peak intensity I_D normalized to NBE intensity I(NBE), denoted as $I_D(\sim2.06$ eV$)/I_{NBE}$ and $I_D(\sim2.50$ eV$)/I_{NBE}$. Both ratios
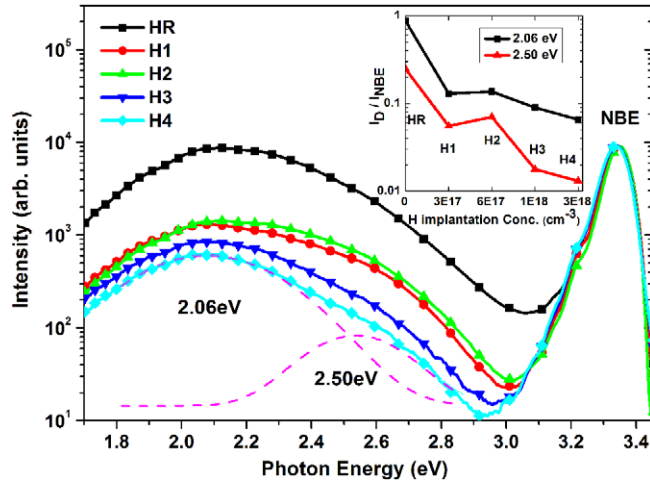
Figure 2. Dose-dependent 80 K $E_B = 5$ keV CL spectra of H-implanted ZnO. H implantation reduces the intensity of V_{Zn} ($\sim$2.06 eV) and V_O ($\sim$2.50 eV). Inset shows the deep band emission decrease with increasing H implantation dose.
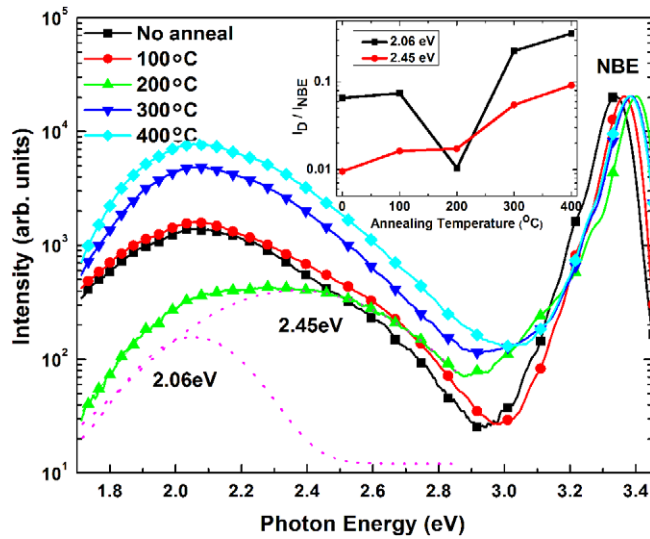

Figure 3. 80 K CL spectra for H-implanted H4-2 after annealing at different temperatures. The inset shows the changes in H4 deep band emission versus post-implant anneal temperature. The 200 °C temperature has the lowest deep band emission.

decrease with increasing H implantation dose (except H2), with the latter decreasing at a faster rate.

Figure 3 provides a comparison of the relative changes of the intensities of deep band emission with the NBE intensity of each spectrum normalized to a constant intensity. With increasing anneal temperature from 100 to 400 °C in 100 °C steps, the deep band emissions of sample H4 first decrease then increase, with the 200 °C anneal having the lowest intensity. This suggests that 200 °C is an optimal temperature for H to minimize the deep band emissions. After annealing HH4 for 30 min, 1 h, 2 h and 4 h at 200 °C, figure 4 shows that the intensity of defect emission first decreases and then increases with annealing time. Each CL spectrum was also normalized at its NBE intensity and it is clear that 1 h anneal leads to the lowest deep band emission. Moreover, with longer annealing time than 1 h, the defect intensity increases. Therefore 1 h is the optimal annealing time to minimize the deep band emissions.
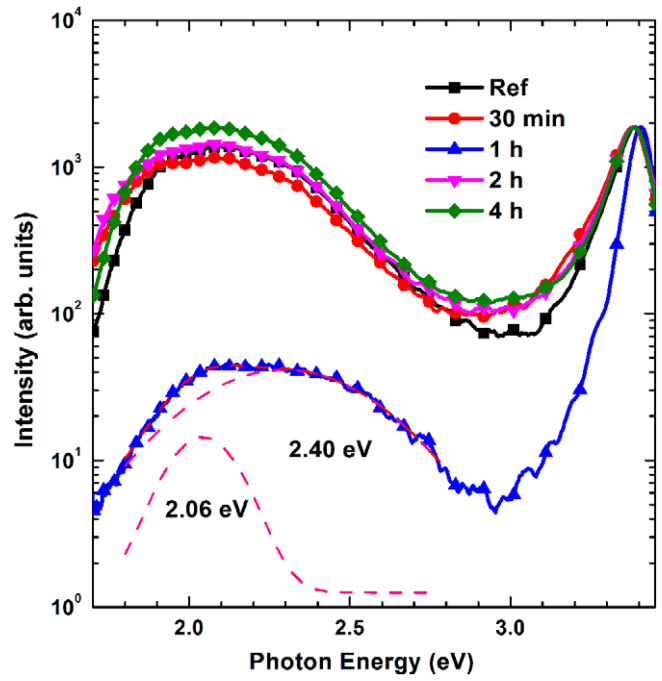

Figure 4. 80 K CL spectra for H-implanted HH4 after annealing at different times at 200 °C. 1 h annealing leads to the lowest deep band emission.

3.2. Electrical properties of H-implanted and annealed ZnO

Tables 1–3 display the results of electrical measurements on H-implanted and annealed ZnO samples H1–H4. They show that annealing temperature has a strong effect on the electrical properties of H-implanted ZnO. HR, H2 and H4 carrier mobilities all reach their maximum values after a 200 °C anneal, then decreased steadily with increasing temperature above 200 °C. This mobility decrease is attributed to increased removal of H from otherwise passivated ionized scattering centres such as Li_{Zn}, V_{Zn} and other defects reported previously [10–12, 29]. For H2 and H4, H passivation can be attributed to the implanted H, while the rather limited passivation of HR could come from 'hidden hydrogen,' identified previously as a hydrogen molecule [40, 41].

Carrier concentrations in table 2 show $\sim$10^4 higher values for H2 versus as-grown HR and 10^2–10^3 higher values for high-dose implanted H4 versus HR. Correspondingly, H2's ρ is much lower than that of HR and H4. This is consistent with the deviation of H2 from the defect emission intensity versus dose trend in figure 2. Note: $\sim$5% of the HT-wafers (Goodwill SPC) have higher than expected n at RT. Tables 2 and 3 show that n for H-implanted H2 and H4 versus anneal temperature exhibits maxima for 300 °C anneal, i.e. 100 °C higher than the temperature for the highest carrier mobility. The TDHE measurements in figure 5 illustrate these differences in n and μ behaviour with annealing temperature. After the 200 °C post-implant anneal, figure 5(a) shows that H4 has the highest carrier mobility, while figure 5(b) shows that n reaches its maximum value after a 300 °C anneal. Section 4 discusses this in detail.

Table 1. RT electrical properties of as-grown HT-ZnO sample HR after annealing in air at the indicated temperatures. Annealing at 200 °C produced the highest μ and n plus the lowest ρ.

Annealing T (°C)	100	200	300	400
μ (cm² V⁻¹ S⁻¹)	109	112	108	106
n (cm⁻³)	7.75×10^{14}	7.83×10^{14}	7.71×10^{14}	7.61×10^{14}
ρ (Ω cm)	74.0	71.4	75.3	77.48

Table 2. RT electrical properties of H-implanted HT-ZnO sample H2 with H box concentration of 6×10^{17} cm⁻³ after annealing in air at different temperatures. Annealing at 200 °C produced the highest μ, nearly the highest n, and the lowest ρ.

Annealing T (°C)	100	200	300	400
μ (cm² V⁻¹ S⁻¹)	146	152	143	127
n (cm⁻³)	9.04×10^{18}	9.0×10^{18}	9.34×10^{18}	7.19×10^{18}
ρ (Ω cm)	0.004 72	0.004 57	0.004 663	0.006 809

Table 3. RT electrical properties of H-implanted HT-ZnO sample H4 with H box concentration of 3×10^{18} cm⁻³ after annealing in air at different temperatures. Annealing at 200 °C produced the highest μ, but annealing at 300 °C produced the highest n, and the lowest ρ.

Annealing T (°C)	100	200	300	400
μ (cm² V⁻¹ S⁻¹)	112	170	149	142
n (cm⁻³)	9.34×10^{15}	4.45×10^{17}	7.30×10^{17}	1.33×10^{17}
ρ (Ω cm)	5.98	0.0823	0.057 43	0.3311

3.3. NBE emission of H-implanted ZnO

The PL spectra in figure 6 show that H4 annealed at 200 °C has the highest NBE emission of all anneal temperatures. The donor bound-exciton transitions at 3.3610 and 3.3617 eV first increase after 200 °C annealing, especially for the peak around 3.3617 eV. With higher annealing temperatures, the peak around 3.3610 eV disappears and the peak around 3.3617 eV decreases more than twice. Previous theory and experiment [42–44] have identified the bound-exciton luminescence at 3.3610 eV as O–H bonds at Zn vacancies, in the form of 4(O–H)–V_{Zn}, which gives rise to shallow donors. The peak around 3.3617 eV could be related to 3(O–H)–V_{Zn}, which is more thermally stable than 4(O–H)–V_{Zn} and has a higher energy transition [42, 44]. After higher temperature annealing, the O–H complexes probably start to disassociate and the H configuration changes, leading to the decrease and shift of this bound-exciton luminescence.

4. Discussion

4.1. H passivation of deep band emission

As can be seen from figures 2 and 3, the deep band emissions all decrease with H implantation. This includes both the V_{Zn} cluster-related defects (∼2.1 eV) and V_O-related defects (∼2.50 eV). Previous research also showed the passivation of deep band emission [10, 11]. Various experiments have demonstrated that the passivation of V_{Zn} by H could involve the neutral Zn vacancy complex $V_{Zn}H_2$ [12, 15, 26], while the passivation of V_O by H could involve a H_O^+ donor [7, 24]. The passivation of O dangling bonds at V_{Zn} by H could form various O–H complexes [42, 44], from 1(O–H)–V_{Zn}, 2(O–H)–V_{Zn}, 3(O–H)–V_{Zn}, to 4(O–H)–V_{Zn}, with 1(O–H)–V_{Zn} as a single

acceptor, 2(O–H)–V_{Zn} as a neutral complex, and the other two as donors.

According to our previous calibration of the DRCLS defect density [28], the $(V_{Zn})_n$ concentration of $(1 - 2) \times 10^{18}$ cm⁻³ in HT-ZnO corresponds to $I_D(\sim 2.06 \text{ eV})/I_{NBE} \sim 1$ in CL spectra. Figure 2 shows $I_D(\sim 2.06 \text{ eV})/I_{NBE} \sim 0.88$ for as-grown HT-ZnO sample, corresponding to a $(V_{Zn})_n$ concentration of $(0.9–1.7) \times 10^{18}$ cm⁻³. Likewise, the concentration of $(V_{Zn})_n$ in the highest H dose implanted H4 corresponds to ∼1.1×10^{17} cm⁻³ after H passivation of Zn vacancy defects.

Figure 3 shows that H reduction of deep level emission and defect passivation are optimal at 200 °C. Moreover, figure 4 indicates that 1 h anneal is the optimal annealing time for H to passivate the defects, corresponding to the lowest CL defect emission. $I_D(\sim 2.06 \text{ eV})/I_{NBE} \sim 0.01$ of H4 after the 1 h 200 °C anneal corresponds to a minimum $(V_{Zn})_n$ concentration of ∼2×10^{16} cm⁻³. At higher temperatures, H passivated defects begin to dissociate. This is consistent with the trap limited diffusion model for implanted H in ZnO, in which implanted H trapped in ZnO will diffuse out starting from 250 °C [31]. The TDHE measurement of highest μ for H4 after a 200 °C anneal in figure 5 is consistent with the implanted H passivating the Li_{Zn}, V_{Zn} and other defects, decreasing the scattering by charged centres and thus increasing the carrier mobility. This effect was also observed on previously annealed hydrogen-implanted HT-ZnO [32].

Li_{Zn} is also an acceptor in HT-ZnO, which shows a CL peak around 3.0 eV [45]. Because of the relatively low Li concentration in these HT-ZnO samples, the Li_{Zn} acceptor could not be detected by our system. However, PAS results of H-implanted ZnO clearly demonstrate the passivation of Li_{Zn} by H; furthermore, H passivates Li_{Zn} before V_{Zn} acceptors [29]. H passivates V_O by forming H_O^+ donors through the following
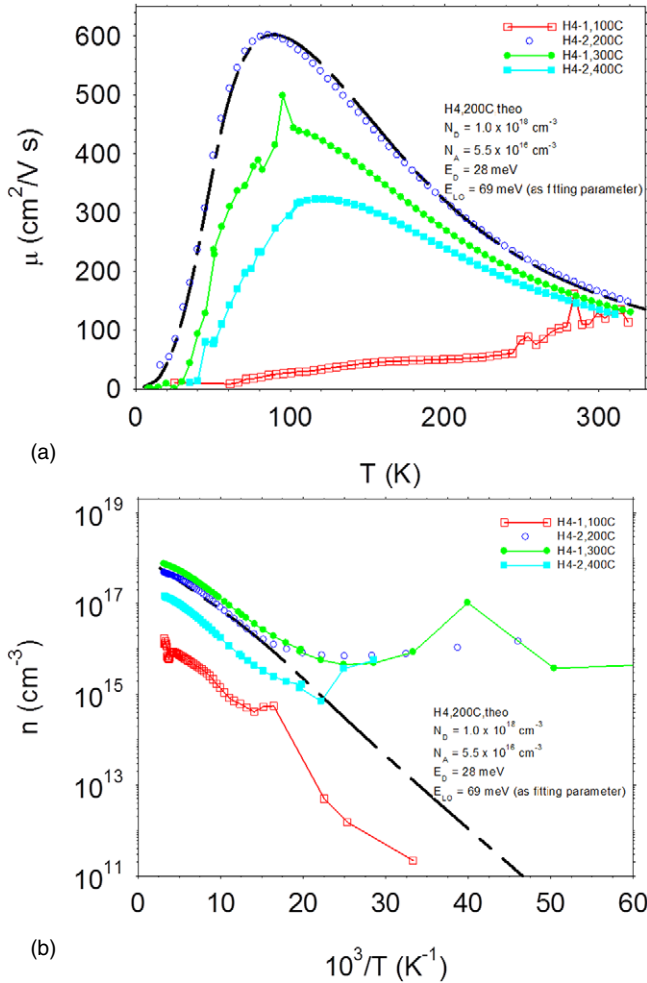
Figure 5. TDHE measurement of H-implanted H4 shows μ (*a*) and n (*b*) versus anneal temperature. The H4 μ reaches a maximum after 200 °C annealing, while n reaches its maximum after 300 °C annealing.

reaction [7]:

$$V_O + H^+ \rightarrow H_O^+. \qquad (1)$$

This is consistent with both (i) figure 2 showing that higher H implantation leads to lower 2.5 eV V_O-related defects and (ii) tables 1–3 showing that n increases with the H implantation. The H_O^+ has been identified as donor bound exciton I$_4$ at 3.3628 eV by PL [24]. Figure 6 indicates this 3.3628 eV peak at a 200 °C anneal. Its relatively low intensity may be due to H passivating the acceptor-like defects before the V_O-related donor-like defects.

4.2. H passivation effect versus donor effect

TDHE measurements of H plasma-treated ZnO film demonstrated that H not only passivates defects and acceptors but also forms shallow donors [46]. Previous research also showed that H in low-defect ZnO samples grown by vapour phase transport will form H_O^+ donors that are detected by PL and labelled I$_4$ [7, 18–21, 24]. For HT ZnO, however, Zn vacancy, O vacancy and Li$_{Zn}$ acceptor defect intensities are relatively high so that implanted H passivation of these defects
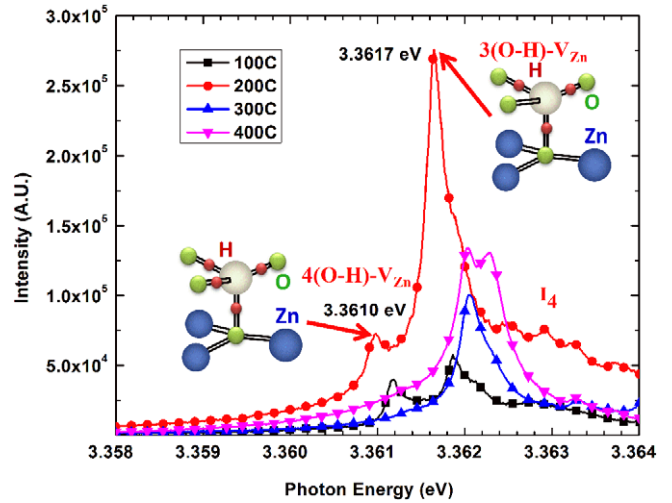

Figure 6. Photoluminescence spectroscopy of H-implanted H4 at low temperatures (4 K). Post-implanted H4 annealed at 200 °C has the highest NBE emission intensity.

before forming donors can account for the low I$_4$ intensity in H-implanted H4.

TDHE measurements support this interpretation. Figure 5(*a*) shows that H4 after a 200 °C anneal reached the highest μ due to H passivating most of the acceptors and other charged scattering centres. Likewise, 5(*b*) shows that H4's n increases to its highest value after the 300 °C anneal due to implanted H passivating V_O and forming shallow H_O^+ donor without dissociating the passivated acceptor defects. However, with more donors, ion scattering increases, thereby decreasing μ. This trend accounts for the n value maximum at a higher anneal temperature than that of the μ value maximum. At higher temperatures, these H passivated complexes begin to dissociate, leaving the initial ionized scattering centre. Other H-implanted ZnO studies have also shown that 200 °C anneal in Ar leads to highest carrier mobility [32, 33], the same as our annealing results in air, demonstrating the consistence of 200 °C as the optimal annealing temperature. It also indicates that at low annealing temperature, below 400 °C as in this study, annealing environment does not affect the annealing effect substantially. Here the 200 °C annealing increases the RT carrier mobility of H4 by ∼1.5× relative to HR. These results show clearly that H passivation of ion scattering centres increases carrier mobility.

This difference in n versus μ annealing behaviour suggests a two-fold process. First, the implanted H passivates the ionized Li$_{Zn}$ [29] and V_{Zn} scattering centres to reduce compensation by these acceptors or to form additional donors. This would allow μ and n to increase with annealing temperature first, especially for H4. Second, V_O complexed with H becomes shallow H_O^+ donors, which increases n further. This increase in n reaches a maximum with the 300 °C anneal. However, the increase in donors will decrease μ because of the ionized impurity scattering. Comparison of HR and H4's n values after 300 °C anneal in tables 1 and 3 shows that H implantation increases n by 3 orders of magnitude, corresponding to the ∼20× decrease in 2.06 eV deep band emission shown in figure 2. The lower n values after higher temperature annealing can be attributed to the reduced H

J. Phys. D: Appl. Phys. **46** (2013) 055107

Z. Zhang *et al*

passivation of acceptors and formation of donors, while the lower μ values is due to a net increase in scattering centres.

4.3. TDHE measurement of donor and acceptor states

The TDHE measurements fitted with $E_{LO} = 69$ meV (details of the fitting procedure can be found elsewhere [47]) in figure 5 show that the donor concentration of approximately 1×10^{18} cm^{-3} for H4-2 200 °C is relatively high compared with the background concentration of other donor impurities in as-grown HT-ZnO such as Al, which is on the order of 10^{17} cm^{-3} [48]. Furthermore, figure 1 shows that the implanted H is about 3×10^{18} cm^{-3}. Therefore, implanted H accounts for the high donor concentration with approximately 30% implanted H activated as donors and the remaining implanted H passivating acceptors and defects.

Figure 5 shows that the donor activation energy is 28 meV [33], close to the activation energy of hydrogen bound in an oxygen vacancy H_O^+, reported previously [9, 23]. IR spectroscopy would be useful to identify the H configuration in these samples; however, its sensitivity is not high enough to study concentrations of about 3×10^{18} H cm^{-3} in layers with a thickness of only 3.5 μm (see, e.g. [24]). The background bulk concentration of H is a few times 10^{17} H cm^{-3} in these samples (500 μm thick) and this will dominate the FTIR spectra. In addition, the acceptor concentration in figure 5 is 5.5×10^{16} cm^{-3}—close to the DRCLS estimate of $\sim 2 \times 10^{16}$ cm^{-3} $(V_{Zn})_n$ density in H4 and consistent with $(V_{Zn})_n$ as the main acceptor after H passivation of Li_{Zn} [29].

As-grown sample HR and H-implanted H2 also showed similar CL, TDH and PL trends as H4 with different annealing temperatures. All of these results indicate that 1 h 200 °C is the optimal annealing condition for H to passivate defects in ZnO and increasing H concentration increases the defect passivation. The implanted H also increases the HT-ZnO carrier mobility and concentration and decreases resistivity by passivating ionized scattering centres, releasing compensated donors and forming H-related donors.

5. Conclusions

This study provides several main conclusions. (1) Implanted H in HT-ZnO decreases deep band V_{Zn}- and V_O-related defect emissions with increasing H dose as H passivates Zn and O vacancies. (2) 1 h annealing at 200 °C is the most effective post-implant anneal condition to passivate deep band defects and increase carrier mobility. (1) The 300 °C anneal activates more shallow donors while preserving acceptor passivation. (4) Annealing at higher temperatures or longer time weakens the passivation effect as implanted H dissociates, increasing deep band emission, lowering carrier mobility, as well as reducing NBE PL emission.

References

[1] Look D C 2001 *Mater. Sci. Eng.* B **80** 383
[2] Pearton S J, Norton D P, Ip L, Heo Y W and Steiner T 2005 *Prog. Mater. Sci.* **50** 293
[3] Look D C, Hemsky J W and Sizelove J R 1999 *Phys. Rev. Lett.* **82** 2552
[4] Janotti A and Van de Walle C G 2007 *Phys. Rev.* B **76** 165202
[5] Zhang S, Wei S-H and Zunger A 2001 *Phys. Rev.* B **63** 075205
[6] Hu J and Gordon R G 1993 *Mater. Res. Soc. Symp. Proc.* **283** 891
[7] Janotti A and Van de Walle C G 2007 *Nature Mater.* **6** 44
[8] Nickel N H and Brendel K 2003 *Phys. Rev.* B **68** 193303
[9] Hofmann M, Hofstaetter A, Leiter F, Zhou H, Henecker F, Meyer B K, Orlinskii S B, Schmidt J and Baranov P G 2002 *Phys. Rev. Lett.* **88** 045504
[10] Sekiguchi T, Ohashi N and Terada Y 1997 *Japan. J. Appl. Phys.* **36** 289
[11] Ohashi N, Ishigaki T, Okada N, Taguchi H, Sakaguchi I, Hishita S, Sekiguchi T and Haneda H 2003 *J. Appl. Phys.* **93** 6386
[12] Lavrov E V, Weber J, Börrnert F, Van de Walle C G and Helbig R 2002 *Phys. Rev.* B **66** 165205
[13] Lee E -C and Chang K J 2004 *Phys. Rev.* B **70** 115210
[14] Wardle M G, Goss J P and Briddon P R 2005 *Phys. Rev.* B **71** 155205
[15] Brauer G, Anwand W, Grambole D, Grenzer J, Skorupa W, Čížek J, Kuriplach J, Procházka I, Ling C C, So C K, Schulz D and Klimm D 2009 *Phys. Rev.* B **79** 115212
[16] Thomas D G and Lander J J 1956 *J. Chem. Phys.* **25** 1136
[17] Van de Walle C G 2000 *Phys. Rev. Lett.* **85** 1012
[18] Cox S F J *et al* 2001 *Phys. Rev. Lett.* **86** 2601
[19] Strzhemechny Y M, Mosbacker H L, Look D C, Reynolds D C, Litton C W, Garces N Y, Giles N C, Halliburton L E, Niki S and Brillson L J 2004 *Appl. Phys. Lett.* **84** 2545
[20] Meyer B K *et al* 2004 *Phys. Status Solidi* b **241** 231
[21] Shi A, Stavola M, Pearton S J, Thieme M, Lavrov E V and Weber J 2005 *Phys. Rev.* B **72** 195211
[22] Monakhov E V, Christensen J S, Maknys K, Svensson B G and Kuznetsov A Yu 2005 *Appl. Phys. Lett.* **87** 191910
[23] Qiu H, Meyer B, Wang Y and Wöll C 2008 *Phys. Rev. Lett.* **101** 236401
[24] Lavrov E V, Herklotz F and Weber J 2009 *Phys. Rev.* B **79** 165210
[25] McCluskey M D, Jokela S J, Zhuravlev K K, Simpson R J and Lynn K G 2002 *Appl. Phys. Lett.* **81** 3807
[26] Bastin D, Lavrov E V and Weber J 2011 *Phys. Rev.* B **83** 195210
[27] McCluskey M D and Jokela S J 2009 *J. Appl. Phys.* **106** 071101
[28] Dong Y, Tuomisto F, Svensson B G, Kuznetsov A Yu and Brillson L J 2010 *Phys. Rev.* B **81** 081201(R)
[29] Johansen K M, Zubiaga A, Tuomisto F, Monakhov E V, Kuznetsov A Yu and Svensson B G 2011 *Phys. Rev.* B **84** 115203

J. Phys. D: Appl. Phys. **46** (2013) 055107

Z. Zhang *et al*

[30] Johansen K M, Christensen J S, Monakhov E V, Kuznetsov A Yu and Svensson B G 2008 *Appl. Phys. Lett.* **93** 152109

[31] Kassier H, Hayes M, Auret F D, Diale M and Svensson B G 2008 *Phys. Status Solidi* c **5** 569

[32] Look D C, Zhang Z, Schifano R, Johansaen K M, Svensson B G and Brillson L J unpublished

[33] Ziegler J F 2008 SRIM, http://www.srim.org

[34] Monakhov E V, Kuznetsov A Yu and Svensson B G 2009 *J. Phys. D: Appl. Phys.* **42** 153001

[35] Katz E J, Zhang Z, Hughes H L, Chung K-B, Lucovsky G and Brillson L J 2011 *J. Vac. Sci. Technol.* B **29** 011027

[36] Brillson L J 2012 *J. Phys. D: Appl. Phys.* **45** 183001

[37] Drouin D, Couture A R, Joly D, Tastet X, Aimez V and Gauvin R 2007 *Scanning* **29** 92

[38] Look D C, Reynolds D C, Sizelove J R, Jones R L, Litton C W, Cantwell G and Harsch W C 1998 *Solid State Commun.* **105** 399

[39] Look D C, Leedy K D, Vines L, Svensson B G, Zubiaga A, Tuomisto F, Doutt D R and Brillson L J 2011 *Phys. Rev.* B **84** 115202

[40] Shi A, Saboktakin M, Stavola M and Pearton S J 2004 *Appl. Phys. Lett.* **85** 5601

[41] Lavrov E V, Herklotz F and Weber J 2009 *Phys. Rev. Lett.* **102** 185502

[42] Lee J-K, Nastasi M, Hamby D W and Lucca D A 2005 *Appl. Phys. Lett.* **86** 171102

[43] Karazhanov S Zh, Marstein E S and Holt A 2009 *J. Appl. Phys.* **105** 033712

[44] Dangbegnon J K, Talla K and Botha J R 2012 *Opt. Mater.* **34** 920

[45] Zhang Z, Knutsen K E, Merz T, Kuznetsov A Yu, Svensson B G and Brillson L J 2012 *Appl. Phys. Lett.* **100** 042107

[46] Cai P F, You J B, Zhang X W, Dong J J, Yang X L, Yin Z G and Chen N F 2009 *J. Appl. Phys.* **105** 083713

[47] Look D C 2005 *Semicond. Sci. Technol.* **20** S55

[48] Vines L, Monakhov E V, Schifano R, Mtangi W, Auret F D and Svensson B G 2010 *J. Appl. Phys.* **107** 103707